Design-Oriented Dissipativity Enhancement for Single-Loop Voltage Control of Grid-Forming VSCs

He, Shan; Blaabjerg, Frede

Published in:
Proceedings of the 2023 IEEE 17th International Conference on Compatibility, Power Electronics and Power Engineering (CPE-POWERENG)

DOI (link to publication from Publisher):
10.1109/CPE-POWERENG58103.2023.10227477

Publication date:
2023

Document Version
Accepted author manuscript, peer reviewed version

Design-Oriented Dissipativity Enhancement for Single-Loop Voltage Control of Grid-FormingVSCs

Shan He
Department of Energy,
Aalborg University
Aalborg, Denmark
she@energy.aau.dk

Frede Blaabjerg
Department of Energy,
Aalborg University
Aalborg, Denmark
fbl@energy.aau.dk

***Abstract*—In light of harmonic stability caused by the control delay and the wide-varied grid impedance, grid-side current feedforward is an effective method to enhance the dissipativity for voltage control of grid-forming converters. However, the dissipative characteristic of converter output impedance is seriously affected by the designed LC-filter resonance frequency and the filter parameters deviation. To fill this gap, a design-oriented control scheme is proposed using three variables feedforward, i.e., converter-side current, capacitor current, and capacitor voltage. As a result, not only the dissipativity can be achieved below Nyquist frequency, but also the dissipativity robustness against the LC-filter parameter deviation is enhanced. Besides, the LC-filter resonance frequency can be designed freely without considering the critical frequency. Finally, the proposed method is validated through the simulation.**

***Keywords*—Grid-forming converters, voltage control, dissipation, LC-filter resonance frequency design, LC-filter parameter deviation.**

I. Introduction

With high penetration of distributed energy resources, grid-forming voltage source converter (VSC) is crucial due to its capability of operating under weak grid or in islanding mode [1-2]. Nevertheless, the grid impedance varies in a wide range, which poses a significant challenge to the harmonic stability of the VSC-grid system. The passivity-based impedance shaping is a promising solution to tackle the instability challenge, and the real part of the output impedance should be non-negative below Nyquist frequency [3-4].

Due to the control delay from the digital pulse width modulation (PWM) process, a non-dissipative region will be induced for single-loop and double-loop voltage control [5]. Grid-side current feedforward (GSCF) is a potential candidate to enhance the dissipativity, but the filter parameter deviation can easily jeopardize the dissipativity around the critical frequency [6]. Further, the LC-filter resonance frequency should be far away from the critical frequency, when considering LC-filter in the internal stability design [7].

In order to overcome the above challenges, a single-loop voltage control scheme is proposed in this paper. The converter-side current feedforward (CSCF), capacitor current feedforward (CCF), and capacitor voltage feedforward (CVF) are used to enhance the dissipativity robustness. Further, the detailed control parameters design is given in terms of the designed LC-filter resonance frequency and the related filter parameter deviation. Finally, simulation results verify the effectiveness of the proposed method.

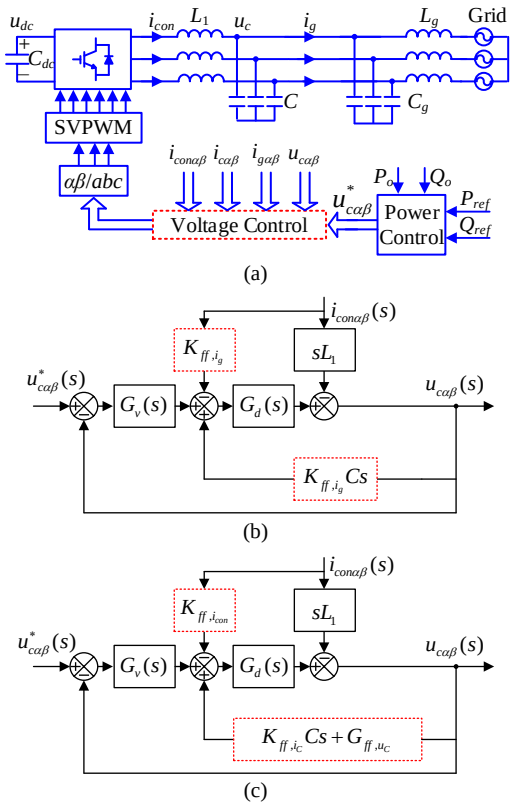

Fig. 1. Single-loop voltage control diagram of a three-phase grid-forming VSC. (a) Three-phase circuit diagram. (b) With grid-side current feedforward. (c) With converter-side current, capacitor current, and capacitor voltage feedforward

II. Modeling and Dissipativity Analysis With/Without Grid-Side Current Feedforward

A. Without grid-side current feedforward

The investigated three-phase grid-forming VSC is depicted in Fig. 1(a), where u_c is the filter capacitor voltage, u_{dc} is the dc-link voltage, i_{con} is the converter-side current, i_c is the filter capacitor current, i_g is the grid-side current, L_1 is the converter-side inductance, C is the filter capacitor. L_g and C_g are the grid impedance, $u^*_{c\alpha\beta}$ is the voltage reference in the $\alpha\beta$-frame.

Considering C as part of the grid impedance, based on Fig. 1(b), the capacitor voltage is

$$u_{c\alpha\beta}(s) = G_{cl}(s)u^*_{c\alpha\beta}(s) - Z_o(s)i^*_{con\alpha\beta} \tag{1}$$

where $G_{cl}(s)$ is the closed-loop transfer function between the reference voltage and the capacitor voltage, $Z_o(s)$ is the converter output impedance seen from the filter capacitor. Their expressions are given as

$$G_{cl}(s)=\frac{G_v(s)G_d(s)}{1+G_v(s)G_d(s)} \tag{2}$$

$$Z_o(s)=\frac{sL_1}{1+G_v(s)G_d(s)}. \tag{3}$$

$G_d(s)$ is the control delay including 1.5 sampling period T_{sa}, which is given as

$$G_d(s)=e^{-1.5sT_{sa}}. \tag{4}$$

Compared to proportional-resonant (PR) controller, R controller is selected for the voltage control as it can extend the voltage control bandwidth [5], which is given as

$$G_v(s)=K_r\frac{s\cos\varphi_g-\omega_g\sin\varphi_g}{s^2+\omega_{rc}s+\omega_g^2}\approx\frac{K_r}{s} \tag{5}$$

where ω_g, ω_{rc}, φ_g, and K_r represent the grid fundamental angle frequency, the cut-off angle frequency of the R controller, the compensation angle of the R controller, and the R controller gain, respectively. According to the passivity theory, a grid-forming VSC can be stabilized if the two constraints are satisfied [3]. First, the closed-loop transfer function $G_{cl}(s)$ should be stable, which can be guaranteed by setting a proper bandwidth. Second, the real part of $Z_o(j\omega)$ is non-negative below Nyquist frequency.

Since the control delay mainly affects the stability in the high-frequency range, the R controller can be simplified as an integrator. Resorting (2), (4) and (5), the open-loop transfer function of voltage control is

$$T_o(s)\approx\frac{K_r}{s}e^{-1.5sT_{sa}}. \tag{6}$$

Then the internal stability can be designed with a given phase margin (PM) φ_m, and the R controller gain is

$$K_r=\omega_c=\frac{0.5\pi-\varphi_m}{T_d}. \tag{7}$$

where ω_c is the cut-off angle frequency of open-loop transfer function of voltage control. Herein, ω_c is set as $\frac{\omega_{sa}}{20}$, and φ_m will be 0.35π, where ω_{sa} is the sampling angle frequency.

By Substituting '$s=j\omega$' into (3), the sign of $Re\{Z_o(j\omega)\}$ is

$$\operatorname{sgn}\left\{\operatorname{Re}\left\{Z_o(j\omega)\right\}\right\}=\operatorname{sgn}\left\{-K_rL_1\cos(\omega T_d)\omega^2\right\}. \tag{8}$$

Based on (8), the dissipative region using single-loop voltage control is

$$f_{dissipative}=(f_{crit},0.5f_{sa}) \tag{9}$$

where the critical frequency is $f_{crit}=1/4T_d$. The dissipative characteristic of single-loop voltage control without grid-side current feedforward is shown in Fig. 2, and the deviation of converter-side inductance only affects the amplitude of $Re\{Z_o(j\omega)\}$ but not the dissipative region. The system specifications of the investigated grid-forming VSC are shown in Table I. In this paper, double-sampling control is used, and the Nyquist frequency is 4000 Hz.

Especially, the designed LC-filter resonance frequency should be larger than the critical frequency, to guarantee the stability for island operation with a zero load. As a result, the filter capacitor should be small enough, which weakens the switching harmonics filtering ability. The same conclusion can be acquired through the open-loop internal stability analysis seen from the PCC point [6-7].

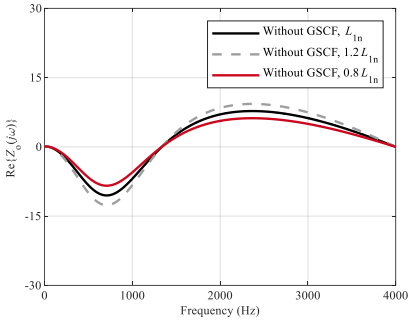

Fig. 2. Dissipative characteristic without grid-side current feedforward.

TABLE I. PARAMETERS OF GRID-FORMING CONVERTER

Symbol	Description	Value	Symbol	Description	Value
P_o	Output power	3.5 kW	u_g	Grid phase voltage (RMS)	110 V
f_{sa}	Sampling frequency	8 kHz	f_{sw}	Switching frequency	4 kHz
L_1	Converter-side inductance	3 mH	C	Filter capacitance	3/15 μF
L_g	Converter-side inductance	3 mH	C_g	Filter capacitance	10 μF

B. With grid-side current feedforward

Proportional GSCF can effectively enhance the dissipativity of voltage control, and the output impedance is

$$Z_o(s)=\frac{sL_1+K_{ff,i_g}G_d(s)}{1+G_v(s)G_d(s)-sCK_{ff,i_g}(s)G_d(s)}. \tag{10}$$

where K_{ff,i_g} is the GSCF coefficient. By substituting '$s=j\omega$' into (10), the sign of $Re\{Z_o(j\omega)\}$ is

$$\operatorname{sgn}\left\{\operatorname{Re}\left\{Z_o(j\omega)\right\}\right\}=\operatorname{sgn}\left\{\begin{matrix}(-K_rL_1+K_{ff,i_g}\\-K_{ff,i_g}L_1C\omega^2)\omega^2\cos(\omega T_d)\end{matrix}\right\}. \tag{11}$$

By changing the sign of $Re\{Z_o(j\omega)\}$ at the critical angle frequency ($2\pi/4T_d$), the proportional GSCF coefficient is

$$K_{ff,i_g}=\frac{K_rL_{1n}}{1-L_{1n}C_n\omega_{crit}^2}=\frac{K_rL_{1n}}{1-\frac{\omega_{crit}^2}{\omega_{rn}^2}}. \tag{12}$$

where L_{1n} and C_n are the nominal values of converter-side inductance and filter capacitance, ω_{rn} is the nominal resonance frequency. Considering a general case of filter parameter deviations, i.e., $L_1=kL_{1n}$, $C=kC_n$, the sign of $\mathrm{Re}\{Z_o(j\omega)\}$ is

$$\operatorname{sgn}\left\{\operatorname{Re}\left\{Z_o(j\omega)\right\}\right\}=\operatorname{sgn}\left\{\begin{matrix}(-K_rkL_{1n}+K_rL_{1n}\frac{1-k^2L_{1n}C_n\omega^2}{1-L_{1n}C_n\omega_{crit}^2})\\\omega^2\cos(\omega T_d)\end{matrix}\right\}. \tag{13}$$

Based on (13), the non-dissipative region using GSCF is

$$f_{non-dissipative}=(f_{crit},\sqrt{\frac{f_{crit}^2}{k^2}+\frac{1-k}{k^2}f_{rn}^2})\text{ or }(\sqrt{\frac{f_{crit}^2}{k^2}+\frac{1-k}{k^2}f_{rn}^2},f_{crit}) \tag{14}$$

As shown in Fig. 3, there are no non-dissipative regions with the nominal filter parameters (k=1). Moreover, −20% parameter deviation can introduce a larger non-dissipative region than +20% deviation, which can also be explained using (14).

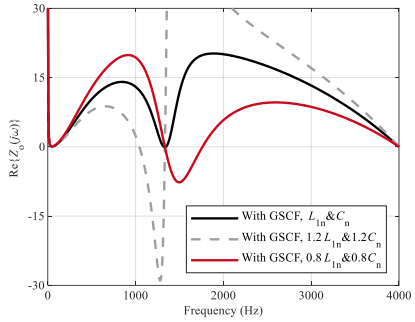

Fig. 3. Dissipative characteristic with grid-side current feedforward when LC-filter resonance frequency is higher than critical frequency (f_{crit}=1333 Hz, f_{rn}=1678 Hz).

On the other hand, the designed LC-filter resonance frequency should be higher than the critical frequency to ensure the dissipativity below Nuquist frequency. Otherwise, there will be no dissipative region, as shown in Fig. 4. Especially, the LC-filter resonance frequency cannot be the same as the critical frequency, because the GSCF coefficient will be infinite according to (12). Further, for island operation with a zero load, K_{ff,i_g} is zero as the load-side current is zero. Then the GSCF cannot contribute to the dissipativity even though $\omega_{rn}>\omega_{crit}$, which is same to single-loop control without feedforward.

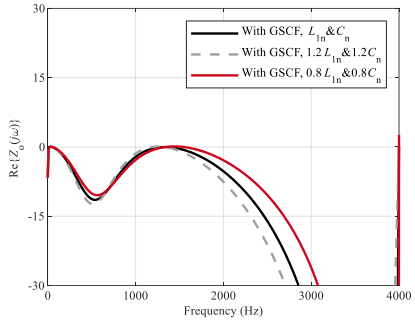

Fig. 4. Dissipative characteristic with grid-side current feedforward when LC-filter resonance frequency is lower than critical frequency (f_{crit}=1333 Hz, f_{rn}=750 Hz).

III. Dissipativity Enhancement

Although GSCF can enhance the dissipativity of voltage control, the damping effects are limited in two aspects. First, the LC-filter resonance frequency should be higher than the critical frequency. Second, the dissipativity can be easily jeopardized by the LC-filter parameter deviation. To overcome the first limit, the GSFC is replaced by the CCF and CSCF. To enhance the dissipativity robustness, a moving-average-filter-based capacitor voltage feedforward (CVF) is superimposed. In addition, the CCF coefficient is optimized according to the required LC-filter parameter deviation. It is worth noting that no extra current sensors are needed compared to GSCF, because the sampled capacitor current can be calculated through the bias between the sampled converter-side current and grid-side current. Moreover, converter-side current sensors are mandatory for over-current protection.

A. *Capacitor current and converter-side current feedforward*

When using CSCF and CCF, the output impedance is

$$Z_o(s)=\frac{sL_1+K_{ff,i_{con}}G_d(s)}{1+G_v(s)G_d(s)-sCK_{ff,i_c}(s)G_d(s)}. \quad (15)$$

where $K_{ff,i_{con}}$ and K_{ff,i_c} are the CSCF coefficient and the CCF coefficient, respectively. By substituting 's=$j\omega$' into (15), the sign of $Re\{Z_o(j\omega)\}$ is

$$\mathrm{sgn}\left\{\mathrm{Re}\left\{Z_o(j\omega)\right\}\right\}=\mathrm{sgn}\begin{Bmatrix}(-K_rL_1+K_{ff,i_{con}}\\-K_{ff,i_c}L_1C\omega^2)\omega^2\cos(\omega T_d)\end{Bmatrix}. \quad (16)$$

By changing the sign of $Re\{Z_o(j\omega)\}$ at the critical angle frequency ($2\pi/4T_d$), the CCF coefficient can be derived as

$$K_{ff,i_c}=\frac{K_{ff,i_{con}}-K_rL_{1n}}{L_{1n}C_n\omega_{crit}^2}. \quad (17)$$

It can be seen from (17) that GSCF is a special case for CSCF and CCF, and (12) can be derived by setting $K_{ff,i_{con}}=K_{ff,i_c}$.In light of passive filter parameter deviations, i.e., L_1=kL_{1n}, C=kC_n, the sign of Re{$Z_o(j\omega)$} is

$$\mathrm{sgn}\left\{\mathrm{Re}\left\{Z_o(j\omega)\right\}\right\}=\mathrm{sgn}\begin{Bmatrix}(-K_rkL_{1n}+K_{ff,i_{con}}-\dfrac{k^2\omega^2}{\omega_{crit}^2}\\(K_{ff,i_{con}}-K_rL_{1n}))\omega^2\cos(\omega T_d)\end{Bmatrix}. \quad (18)$$

To ensure the dissipativity under an ideal case (k=1), the constraint to the CSCF coefficient is

$$K_{ff,i_{con}}\geq K_rL_{1n}. \quad (19)$$

The dissipative characteristic with different values of $K_{ff,i_{con}}$ is depicted in Fig. 5. Consequently, the dissipativity is not limited by the designed LC-filter resonance frequency. Moreover, a larger CSCF coefficient is beneficial to the dissipativity, and $K_{ff,i_{con}}$ is set as $\frac{\omega_{sa}L_{1n}}{10}$ in the following analysis.

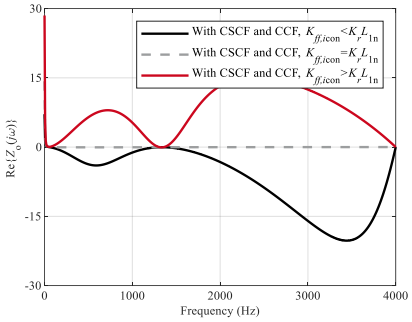

Fig. 5. Dissipative characteristic with converter-side current and capacitor current feedforward considering different converter-side current feedforward coefficient ($K_r=\frac{\omega_{sa}}{20}$, $K_{ff,i_{con}}=\frac{\omega_{sa}L_{1n}}{40},\frac{\omega_{sa}L_{1n}}{20},\frac{\omega_{sa}L_{1n}}{10}$).

Recalling (18), the non-dissipative region when L_1=kL_{1n}, C=kC_n is given in (20). As shown in Fig. 6, a −20% parameter deviation can introduce a larger non-dissipative region than a +20% deviation.

$$f_{non-dissipative}=\left(f_{crit},\frac{f_{crit}}{k}\sqrt{\frac{K_{ff,i_{con}}-K_rL_{1n}k}{K_{ff,i_{con}}-K_rL_{1n}}}\right)$$
$$\text{or }\left(\frac{f_{crit}}{k}\sqrt{\frac{K_{ff,i_{con}}-K_rL_{1n}k}{K_{ff,i_{con}}-K_rL_{1n}}},f_{crit}\right) \quad (20)$$

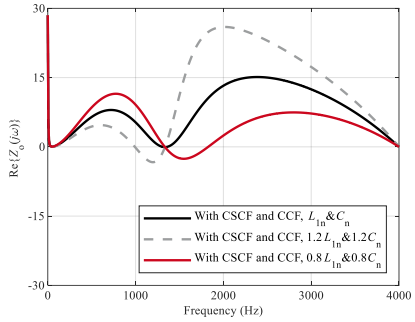

Fig. 6. Dissipative characteristic with converter-side current feedforward and capacitor current feedforward considering LC-filter parameter deviations ($K_r = \frac{\omega_{sa}}{20}$ and $K_{ff,i_{con}} = \frac{\omega_{sa} L_{1n}}{10}$).

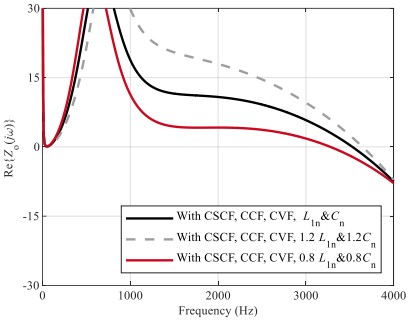

Fig. 7. Dissipative characteristic with converter-side current feedforward, capacitor current feedforward, and proportional capacitor voltage feedforward ($K_{ff,u_c} = 0.5$).

B. *Capacitor current, converter-side current, and proportional capacitor voltage feedforward*

CVF is commonly used in the current control of grid-following converters to enhance the dissipativity robustness [8], and the converter output impedance is

$$Z_o(s) = \frac{sL_1 + K_{ff,i_{con}} G_d(s)}{1 + G_v(s)G_d(s) - sCK_{ff,i_c}(s)G_d(s) - G_{ff,u_c}G_d(s)}. \tag{21}$$

where G_{ff,u_c} is the CVF function. The most direct method is proportional CVF, which is given as

$$G_{ff,u_c} = K_{ff,u_c} \tag{22}$$

By substituting '$s=j\omega$' and (22) into (21), the sign of $Re\{Z_o(j\omega)\}$ considering CCF, CSCF, and proportional CVF is

$$\mathrm{sgn}\left\{\mathrm{Re}\left\{Z_o(j\omega)\right\}\right\} = \mathrm{sgn}\begin{Bmatrix} (-K_r L_1 + K_{ff,i_{con}} - K_{ff,i_c} L_1 C\omega^2) \\ \omega^2 \cos(\omega T_d) + (L_1 \sin(\omega T_d)\omega \\ -K_{ff,i_{con}})K_{ff,u_c}\omega^2 \end{Bmatrix}. \tag{23}$$

Then the dissipative characteristic of converter output impedance at the critical frequency is

$$\mathrm{sgn}\left\{\mathrm{Re}\left\{Z_o(j\omega_{crit})\right\}\right\} = \mathrm{sgn}\left\{(\omega_{crit} k L_{1n} - K_{ff,i_{con}})K_{ff,u_c}\omega_{crit}^{\ 2}\right\}. \tag{24}$$

Hence, the allowed maximum negative filter parameter deviation is

$$k \geq \frac{K_{ff,i_{con}}}{\omega_{crit} L_{1n}} \tag{25}$$

Recalling (4), the minimum value of k is 0.6 when $K_{ff,i_{con}} = \frac{\omega_{sa} L_{1n}}{10}$. As illustrated in Fig. 7, the dissipativity robustness against the passive filter deviation near the critical frequency can be enhanced with the CVF. However, another non-dissipative region around the Nyquist angle frequency is introduced. The dissipative characteristic at the Nyquist frequency is

$$\mathrm{sgn}\left\{\mathrm{Re}\left\{Z_o(j0.5\omega_{sa})\right\}\right\} = \mathrm{sgn}\begin{Bmatrix} -(0.5\omega_{sa} k L_{1n} + K_{ff,i_{con}}) \\ K_{ff,u_c}\, 0.25\omega_{sa}^{\ 2} \end{Bmatrix} < 0. \tag{26}$$

Note that the internal stability in (2) and (6) should be paid attention especially when adding CVF, and the open-loop transfer function in (6) is modified as

$$T_{o1}(s) \approx \frac{K_r e^{-1.5sT_{sa}}}{s(1-(K_{ff,i_c} Cs + K_{ff,u_c})e^{-1.5sT_{sa}})}. \tag{27}$$

Within the voltage control bandwidth, the delay and the derivative terms in (27) can be ignored. Then, (27) is further simplified as

$$T_{o2}(s) \approx \frac{K_r e^{-1.5sT_{sa}}}{s(1-K_{ff,u_c})}. \tag{28}$$

As a result, (7) is modified as

$$K_r = \omega_c (1 - K_{ff,u_c}). \tag{29}$$

The bode diagram of open-loop transfer function with and without simplification is shown in Fig. 8. It can be found that the amplitude-frequency characteristic is almost the same without and with simplification, which validates the effectiveness of (29).

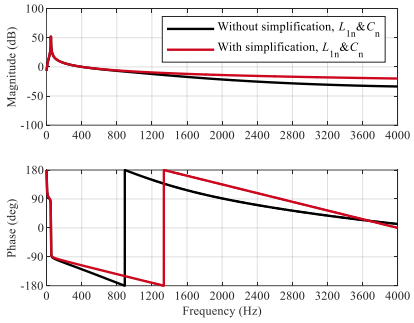

Fig. 8. Bode diagram of open-loop transfer function with and without simplification ($K_{ff,u_c} = 0.5$).

C. *Capacitor current, converter-side current, and moving-average-filter-based capacitor voltage feedforward*

When using proportional CVF, the non-dissipative region around the Nyquist frequency is mainly caused by '$\sin(0.5\omega_{sa}1.5T_{sa})$' in (23) and (26). To remove this region, an extra $0.5T_{sa}$ delay can be added in the CVF path, i.e., '$\sin(0.5\omega_{sa}2T_{sa})$' becomes zero at the Nyquist frequency. In the practical implementation, a moving average filter (MAF) is used in the CVF path, which is

$$G_{ff,u_c}(s) = K_{ff,u_c}(0.5 + 0.5e^{-sT_{sa}}). \tag{30}$$

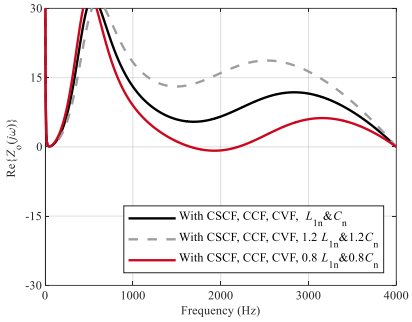

Fig. 9. Dissipative characteristic with converter-side current feedforward, capacitor current feedforward, and moving-average-filter-based capacitor voltage feedforward ($K_{ff,u_c}=0.5$).

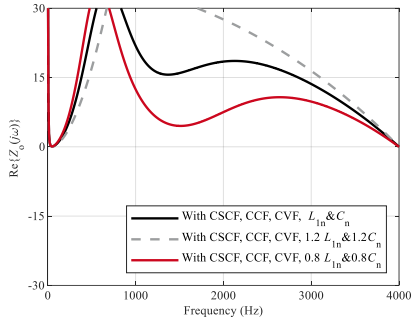

(a)

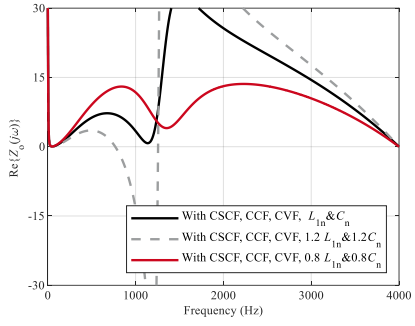

(b)

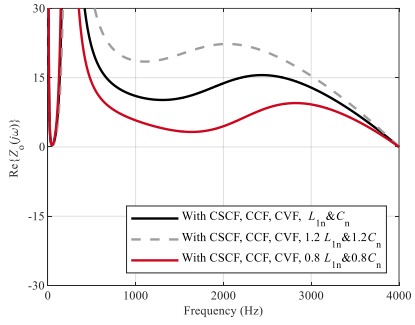

(c)

Fig. 10. Dissipative characteristic with converter-side current feedforward, corrected capacitor current feedforward, and moving-average-filter-based capacitor voltage feedforward. (a) $K_{ff,u_c}=0.5$, (b) $K_{ff,u_c}=0.1$, (c) $K_{ff,u_c}=0.9$.

Compared to Fig. 7, the dissipativity around the Nyquist frequency is enhanced, but another non-dissipative region is introduced with a –20% LC-filter parameter deviation (see Fig. 9). Further, a CCF correction term considering negative parameter deviation is added to enhance the dissipativity, which is given as

$$K_{ff,i_c}=\frac{K_{ff,i_{con}}-K_r L_{1n} m}{L_{1n} C_n m^2 \omega_{crit}^2}. \tag{31}$$

Specifically, m is set to 0.8 considering a −20% parameter deviation. In addition, m can be designed to lower values in terms of the larger parameter deviation. Interestingly, the dissipativity can be still achieved under a +20% parameter deviation when m is 0.8, as shown in Fig. 10 (a).

On the other hand, the dissipativity will be weakened when $K_{ff,u_c}=0.1\ or\ 0.9$, as shown in Fig. 10(b)-(c). Moreover, it can be seen from Fig. 11 that a larger K_{ff,u_c} will limit the voltage control bandwidth. Hence, K_{ff,u_c} is set as 0.5 in terms of the voltage control bandwidth and the dissipativity robustness. As the CVF coefficient has an obvious effect on the low-frequency dissipativity, it will be further investigated by combining the power control loop.

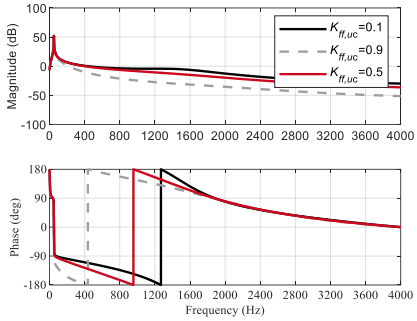

Fig. 11. Bode diagram of open-loop transfer function with converter-side current feedforward, corrected capacitor current feedforward, and moving-average-filter-based capacitor voltage feedforward.

IV. Case Study

A. *Effect of LC-filter parameter design on dissipativity*

To investigate the limitation of LC-filter parameter design on the dissipativity, the LC-filter resonance frequency (750 Hz) is set as lower than the critical frequency (1333 Hz). Regarding the filter capacitance as part of grid impedance, the equivalent grid impedance is $Z_{g,eq}(s)=\frac{sL_g}{1+s^2L_g(C+C_g)}$. It can be seen from Fig. 12 that $Z_o(s)$ intersects with $Z_{g,eq}(s)$ in the negative-real-part region, which leads to a −20.8° PM and destabilizes the system. The related simulation results are given in Fig. 13, where the VSC starts at 20 ms and the power reference is set as zero. As shown in Fig. 13, only using GSCF cannot stabilize the system and the proposed method can always remain dissipative.

B. *Effect of LC-filter parameter deviation on dissipativity*

Even though the LC-filter resonance frequency (1678 Hz) is higher than the critical frequency (1333 Hz), the dissipativity around the critical frequency is weak with GSCF. Considering a −20% deviation of nominal values of L_1 and C, as shown in Fig. 14, the system still cannot be stabilized for the GSCF (PM=−36.3°). After implementing the proposed method, the system becomes stable and the PM is 4.4°, as shown in Fig. 14 and Fig. 15.

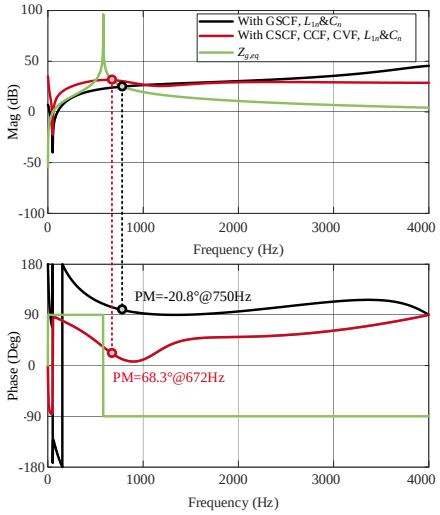

Fig. 12. VSC output impedance $Z_o(s)$ seen from the capacitor (C=15 μF) with L_g=3 mH and C_g=10 μF.

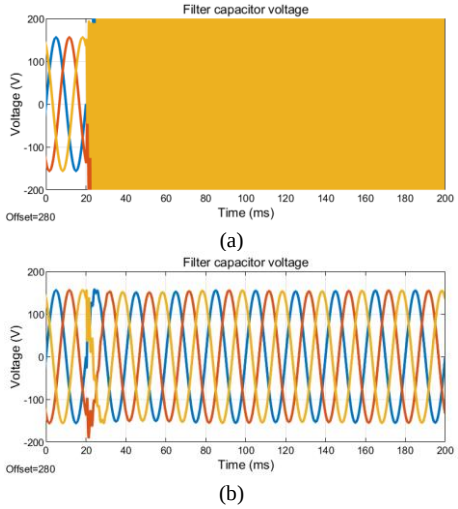

Fig. 13. Dissipativity assessment when LC-filter resonance frequency is lower than critical frequency (f_{rn}=750 Hz, f_{crit}=1333 Hz, L_g=3 mH, C_g=10 μF). (a) With grid-side current feedforward. (b) Proposed method.

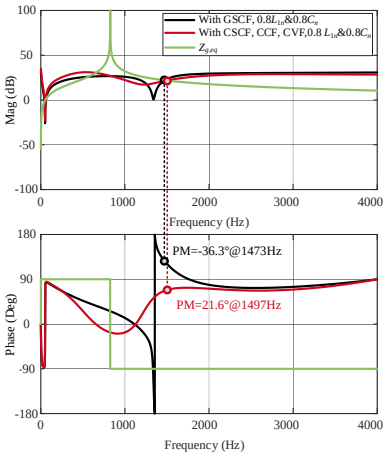

Fig. 14. VSC output impedance $Z_o(s)$ seen from the capacitor (C=3 μF) with L_g=3 mH and C_g=10 μF.

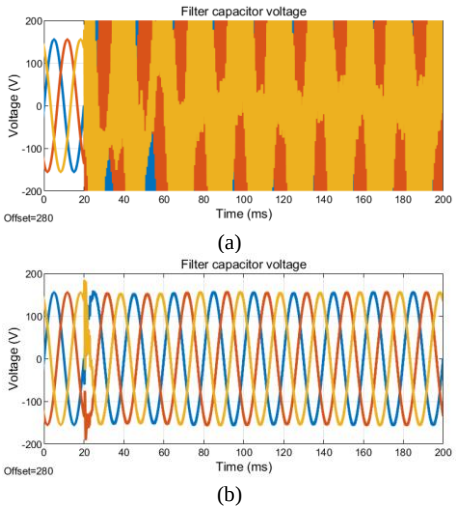

Fig. 15. Simulation results with a −20% deviation of L_1 and C (f_{rn}=1678 Hz, f_{crit}=1333 Hz, L_g=3 mH, C_g=10 μF). (a) With grid-side current feedforward. (b) Proposed method.

V. Conclusion

This paper first investigates the dissipativity for LC-filtered grid-forming VSCs with grid-side current feedforward, and the LC-filter resonance frequency should be designed higher than the critical frequency. Further, the dissipativity around the critical frequency is vulnerable in terms of LC-filter parameter deviation. To tackle the challenge of the LC-filter design, the grid-side current feedforward is replaced by the converter-side current feedforward and the capacitor current feedforward. To enhance the dissipativity robustness against parameter deviation, a correction term is added in the capacitor current feedforward. In addition, a moving-average-filter-based capacitor voltage feedforward is superimposed. As a result, the dissipative region is optimized to Nyquist frequency, and the dissipativity robustness is enhanced at the same time. Finally, the proposed method is validated through simulation.

References

[1] R. H. Lasseter, Z. Chen, and D. Pattabiraman, "Grid-forming inverters: A critical asset for the power grid," *IEEE J. Emerg. Sel. Top. Power Electron.*, vol. 8, no. 2, pp. 925–935, Jun. 2020.

[2] R. Rosso, X. Wang, M. Liserre, X. Lu, and S. Engelken, ''Grid-forming converters: control approaches, grid-synchronization, and future trends—A review,'' *IEEE Open J. Ind. Appl.*, vol. 2, pp. 93–109, 2021.

[3] L. Harnefors, X. Wang, A. Yepes, and F. Blaabjerg, "Passivity-based stability assessment of grid-connected VSCs-An overview," *IEEE J. Emerg. Sel. Top. Power Electron.*, vol. 4, no. 1, pp. 116–125, Mar. 2016.

[4] L. Harnefors, A. Yepes, A. Vidal, and J. Doval-Gandoy, "Passivity-based controller design of grid-connected VSCs for prevention of electrical resonance instability," *IEEE Trans. Ind. Electron.*, vol. 62, no. 2, pp. 702–710, Feb. 2015.

[5] Y. Liao, X. Wang, and F. Blaabjerg, "Passivity-based analysis and design of linear voltage controllers for voltage-source converters," *IEEE Open J. Ind. Electron. Soc.*, vol. 1, pp. 114–126, June 2020.

[6] G. Wu, Y. He, H. Zhang, X. Wang, D. Pan, X. Ruan, and C. Yao, "Passivity-based stability analysis and generic controller design for grid-forming inverter," *IEEE Trans. Power Electron.*, *early access*, 2023.

[7] X. Wang, P. C. Loh, and F. Blaabjerg, "Stability analysis and controller synthesis for single-loop voltage-controlled VSIs," *IEEE Trans. Power Electron.*, vol. 32, no. 9, pp. 7394–7404, Sep. 2017.

[8] C. Xie, K. Li, J. Zou, and J. Guerrero, "Passivity-based stabilization of LCL-type grid-connected inverters via a general admittance model," *IEEE Trans. Power Electron.*, vol. 35, no. 6, pp. 6636-6648.